Science of the Total Environment 847 (2022) 157503

Contents lists available at ScienceDirect

Science of the Total Environment

journal homepage: www.elsevier.com/locate/scitotenv

Understanding source terms of anthropogenic uranium in the Arctic Ocean – First ^{236}U and ^{233}U dataset in Barents Sea sediments

Jixin Qiao [a,*], Hilde Elise Heldal [b], Peter Steier [c]

[a] Department of Environmental and Resource Engineering, Technical University of Denmark, DTU Risø Campus, DK-4000 Roskilde, Denmark
[b] Department of Contaminants and Biohazards, Institute of Marine Research, P.O.Box 1870 Nordnes, NO-5817 Bergen, Norway
[c] VERA Laboratory, Faculty of Physics – Isotope Research, University of Vienna, Währinger Straße 17, A-1090 Vienna, Austria

HIGHLIGHTS

- First dataset of ^{236}U and ^{233}U in Barents Sea sediment profiles
- Source terms of anthropogenic uranium in western Barents Sea were identified.
- Global fallout is the predominate sources in sediments of the study region.
- Local nuclear legacies unlikely contributed significant anthropogenic uranium.
- ^{236}U-^{233}U can be potential benchmarks in age-depth model for sediment dating.

GRAPHICAL ABSTRACT

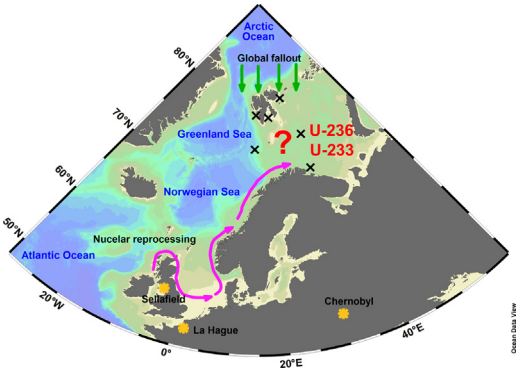

ARTICLE INFO

Editor: Filip M.G. Tack

Keywords:
^{233}U
^{236}U
Barents Sea
Sediment
Source term
Dating

ABSTRACT

This work reports the first dataset of ^{236}U and ^{233}U in sediment cores taken from the Barents Sea, with the aim to better understand the source terms of anthropogenic uranium in the Arctic region. Concentrations of ^{236}U and ^{233}U along with ^{137}Cs, and $^{233}U/^{236}U$ atomic ratio were measured in six sediment profiles. The cumulative areal inventories of ^{236}U and ^{233}U obtained in this work are (3.50–12.7) $\times 10^{11}$ atom/m^2 and (4.92–21.2) $\times 10^{9}$ atom/m^2, with averages values of (8.08 ± 2.93) $\times 10^{11}$ atom/m^2 and (1.08 ± 0.56) $\times 10^{10}$ atom/m^2, respectively. The total quantities of ^{236}U and ^{233}U deposited in the Barents Sea bottom sediments were estimated to be 507 ± 184 g and 7 ± 3 g, respectively, which are negligible compared to the total direct deposition of ^{236}U (6000 g) and ^{233}U (40–90 g) from global fallout in the Barents Sea. The integrated atomic ratios of $^{233}U/^{236}U$ ranging in (0.98–1.57) $\times 10^{-2}$ reflect the predominant global fallout signal of ^{236}U in the Barents Sea sediments and the highest reactor-^{236}U contribution accounts for 30 ± 14 % among the six sediment cores. The reactor-^{236}U input in the Barents Sea sediments is most likely transported from the European reprocessing plants rather than related to any local radioactive contamination. These results provide better understanding on the source term of anthropogenic ^{236}U in the Barents Sea, prompt the oceanic tracer application of ^{236}U for studying the dynamics of the Atlantic-Arctic Ocean and associated climate changes. The ^{236}U-^{233}U benchmarked age-depth profiles seem to match reasonably well with the reported input function history of radioactive contamination in the Barents Sea, indicating the high potential of anthropogenic ^{236}U-^{233}U pair as a useful tool for sediment dating.

* Corresponding author.
E-mail address: jiqi@dtu.dk (J. Qiao).

http://dx.doi.org/10.1016/j.scitotenv.2022.157503
Received 20 April 2022; Received in revised form 15 July 2022; Accepted 15 July 2022
Available online 22 July 2022

1. Introduction

In the recent decade, ^{236}U ($t_{½}$ = 2.34 × 10^7 y) has been recognized as a promising oceanic tracer and successfully applied to investigate circulation pathways and timescales in the world oceans (Casacuberta et al., 2016; Castrillejo et al., 2018; Villa-Alfageme et al., 2019; Wefing et al., 2019). In contrast to its natural production, for which the global inventory is about 35 kg, >1000 kg of ^{236}U in the environment is of anthropogenic origin and was released via human nuclear activities. The primary sources of anthropogenic ^{236}U include global fallout (about 900–1400 kg) of atmospheric nuclear weapons testing (Sakaguchi et al., 2009; Steier et al., 2008; Winkler et al., 2012) and discharges (about 250 kg) from the two European nuclear fuel reprocessing plants at Sellafield (SF) and La Hague (LH) (Castrillejo et al., 2020). In addition, releases from nuclear accidents (e.g., Chernobyl accident) (Lin et al., 2021) and local sources (e.g., Studsvik research facility) (Qiao et al., 2021) made minor contributions.

Though ^{236}U released from different sources are expected to have characteristic $^{236}U/^{238}U$ isotopic ratios, the ubiquity of natural ^{238}U alters the $^{236}U/^{238}U$ ratios and makes it difficult to distinguish ^{236}U source terms in the environment (Qiao et al., 2017). Very recently, advances in the accelerator mass spectrometry (AMS) technique open up the possibility to determine another anthropogenic uranium isotope ^{233}U ($t_{½}$ = 1.59 × 10^5 y) at environmental levels (Hain et al., 2020). This enables the application of ^{233}U-^{236}U pair to identify the origin of ^{236}U (Hain et al., 2020; Lin et al., 2021; Lin et al., 2022b; Qiao et al., 2022; Qiao et al., 2021; Qiao et al., 2020), because the $^{233}U/^{236}U$ ratios, only replying to the burn-up history of the nuclear fuel, are not altered by the biogeochemical processes along the transport pathways.

The production of ^{233}U is mostly by fast neutrons via ^{235}U (n,3n) ^{233}U reaction or directly by ^{233}U-fueled devices in nuclear weapons tests, and nearly no ^{233}U can be produced in civil nuclear facilities such as thermal power reactors or reprocessing plants (Hain et al., 2020). The integrated $^{233}U/^{236}U$ atomic ratio for global fallout signal in the ocean was estimated to be (1.40 ± 0.15) × 10^{-2} after the termination of atmospheric nuclear weapons testing in the 1980s (Hain et al., 2020), whereas sources associated with the civil nuclear industry were at the level of 1 × 10^{-7}-1 × 10^{-6} (HELCOM MORS Discharge database, n.d.; Naegeli, 2004). It should be noted that due to different source inputs between ^{233}U and ^{236}U from the atmospheric weapons testing, $^{233}U/^{236}U$ atomic ratios higher than the integrated value of (1.40 ± 0.15) × 10^{-2} have been reported for global fallout during 1950s–1970s in regional natural archives (Hain et al., 2020; Lin et al., 2021; Qiao et al., 2022).

The Barents Sea is a shelf sea with an average depth of 230 m and a total area of 1.6 million km^2 (Carmack et al., 2006). It is bordered by Svalbard to the northwest, Franz Josef Land to the northeast, Novaya Zemlya to the east and the coast of northern Norway and Russia to the south (Fig. 1). The 500-m depth isobath delimits the Barents Sea towards the west and the polar basins in the north (Johannesen et al., 2012). The Barents Sea consists of three main types of water masses (Loeng, 1991): 1) warm, saline Atlantic water (temperature > 3 °C, salinity >35) from the North Atlantic Current (NAC); 2) cold Arctic water (temperature < 0 °C, salinity <34.3–34.8) from the north; and 3) warm, but not very salty coastal

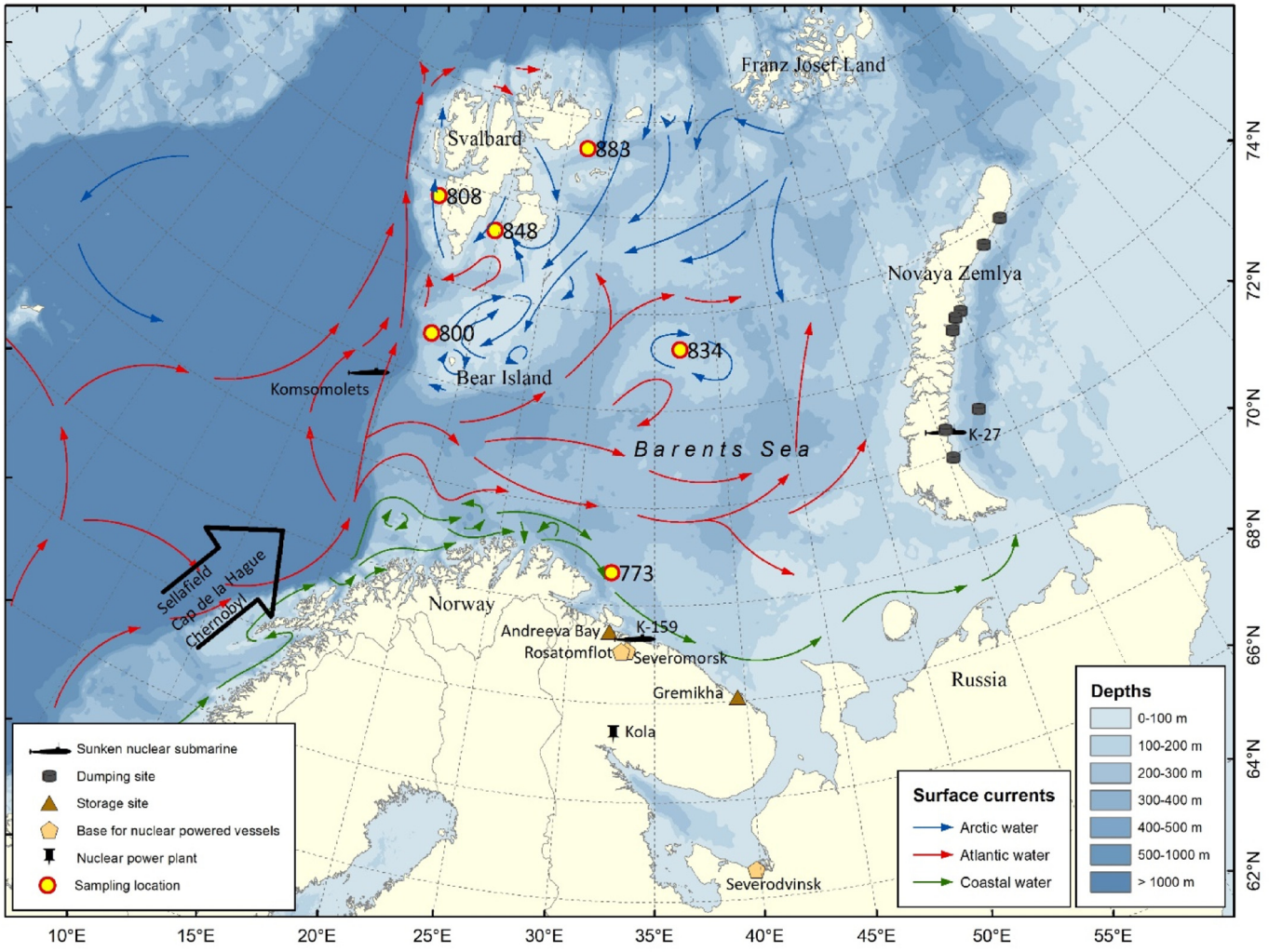

Fig. 1. Main surface currents and water transport systems in the Barents Sea region and sampling locations of sediment cores in this work.

water (temperature > 2 °C, salinity <34.7). Northward-flowing ocean currents transport warm Atlantic water eastwards and northwards into Arctic Ocean, whereas southward-flowing ocean currents transport cold Arctic water southwards back to the Barents Sea.

It is well known that sediments may act as a repository for a variety of contaminants including radionuclides (Durrant et al., 2018; Knies et al., 2006; Muz et al., 2020; Zaborska et al., 2011). Sediments with high content of clay minerals (e.g. smectite) and rich in organic carbon have the highest repository potential (Knies et al., 2006). Knowledge about sediment characteristics and dispersal in the marine environment is important to understand variations in the radionuclide content in sediments. The process of sedimentation is controlled by physiogeographic parameters like distance to shore, seabed bathymetry and ocean currents (Knies et al., 2006; Knies and Martinez, 2009). Coarse-grained sediments are mainly deposited in coastal zones, whereas fine-grained sediments are transported and deposited in deeper water. Further, shallow banks have generally little sedimentation of finer sediments due to strong ocean currents. Sedimentation along the marginal ice zone in the northern Barents Sea is also affected by physical and ecological processes related to sea ice coverage and melting (Falk-Petersen et al., 2000; Falk-Petersen et al., 1998). Sea ice may carry contamination particles that may be released during ice melting. During winter, sea ice formed in the Kara Sea travels around the northern tip of Novaya Zemlya and into the Barents Sea south of Franz Josef Land, further southwest towards Svalbard and Spitsbergen (Dethleff et al., 2000; Heldal et al., 2002; VIinje and Kvambekk, 1991). Contamination from the Kara Sea, which has several dumping sites for radioactive wastes (AMAP, 2015), can thus be transported to the marginal ice zone in the Barents Sea.

Anthropogenic radionuclides entered the Barents Sea during the atmospheric nuclear weapons testing in 1945–1980 through both global (stratospheric) fallout and regional (tropospheric) fallout primarily from the Novaya Zemlya test site (Smith et al., 1995; UNSCEAR, 2000). The Norwegian Coastal Current (NCC) and Atlantic water also transport radioactive substances released from the Chernobyl accident, SF and LH northwards into the Barents Sea and the Arctic Ocean (Brown et al., 2002; Kershaw and Baxter, 1995; Kershaw et al., 2004; Kershaw et al., 1999). Besides, radioactive releases from the operation of local nuclear installations, submarine incidents (e.g. Komsomolets) and waste dumping activities (Novaya Zemlya) have also contributed to the total inventory of radioactivity in the Barents Sea (AMAP, 2015; Baxter et al., 1995; Gwynn et al., 2016). The Barents Sea is also surrounded by industrial and defense enterprises, and by sea and river ports that are used to transport nuclear materials and radioactive substances (Yakovlev and Puchkov, 2020). These are potential sources of radioactive contamination.

Our earlier works have demonstrated the power of $^{233}U/^{236}U$ as a sensitive fingerprint for distinguishing reactor sources from the fallout of atmospheric nuclear weapons testing in complex marine systems (Qiao et al., 2021; Qiao et al., 2020). Therefore, in this work, we aim to explore the ^{233}U-^{236}U paired tracer to understand the sources, levels and transport passages of anthropogenic uranium in the Barents Sea and to reveal the impact of historical radioactive releases and local nuclear activities on the marine environment. Six sediment cores were sampled in the Barents Sea, and analysed for ^{236}U and ^{233}U, along with ^{238}U and ^{137}Cs, to obtain insights into both geographical variations (spatial variations) and changes as a function of time (temporal variations).

2. Material and methods

2.1. Sample collection and preparation

Six sediment cores were collected onboard R/V "Johan Hjort" in August–September 2015 using a "Smøgen" box corer (30 × 30 cm inner dimensions). The cores were collected using PVC tubes (10 cm i. d. × 40 cm length). They were cut into 1 cm slices between the depth of 0–10 cm, and 2 cm slices from 10 cm to the bottom onboard the ship. The samples were stored at −20 °C until further preparation took place at Institute of Marine Research (IMR), Bergen, Norway. At IMR, the samples were freeze-dried using a CHRIST ALPHA 1–4 freeze dryer until the constant dry weight was achieved. The samples were homogenized using a Retsch Planetary Ball Mill PM 100.

Seawater temperature and salinity were measured at all sampling sites using a SeaBird Electronics SBE911 CTD (Conductivity-Temperature-Depth) profiler mounted on a General Oceanics rosette carousel equipped with 12 of 2.5 L Niskin bottles.

2.2. Sampling sites

The sampling locations are shown in Fig. 1 and details on each sampling site are summarized in Table 1. Seabed information near the sites is summarized below according to the Mareano mapping of the Barents Sea (www.mareano.no).

Station 773 is located within the NCC close to the Norwegian coast. This station is the one with the highest surface seawater temperature (10.45 °C). The salinity of surface seawater at this station (34.23) is affected by inputs of freshwater from land. Due to the transport of radioactive contamination with the NCC, slightly higher levels of ^{137}Cs were found in this area compared to other parts of the Barents Sea (Skjerdal et al., 2020). The seabed near the station is gravelly sand.

Station 800 is located at the northwest of Bear Island. Based on temperature and salinity in surface and bottom water (Table 1), it is clear that the seawater at this station largely consists of Atlantic water. This area may, however, be affected by Arctic water flowing in from the north (Loeng, 1991). Sediments in the area adjacent to station 800 contain mainly gravelly sand.

Station 808 is located within the ice melting zone at the west coast of Spitsbergen in the Svalbard Coastal Current, which is a continuation of the East Spitsbergen Current. The salinity of the surface seawater shows a large degree of Arctic character. The seabed in the surrounding area of the station consists of sandy gravel/mud and sand with gravel, stone and block.

Station 834 is located at the relatively shallow Central Bank in the Barents Sea. The dominating water mass at the surface is likely a mixture of inflowing Atlantic water and seasonally heated meltwater. This is confirmed by temperature of 5.70 °C and salinity of 34.87. The temperature and salinity of bottom seawater are 0.57 °C and 35.03, implying it is a mixture of Atlantic water cooled during winter and/or possibly mixed with cold, high-salinity water from ice freezing and brine release during winter. Sediments at station 834 contain mud and sand with gravel, stone and block.

Station 848 is located in the Storfjorden at Spitsbergen. The dominant water mass here is the East Spitsbergen Current with characteristics of Arctic water. The temperature in surface and bottom seawater is 1.27 and −1.83 °C, respectively, and salinities in surface and bottom seawater are 33.45 and 35.05, respectively. The extremely cold and saline bottom water is quite common in Storfjorden because of ice freezing and brine release during winter (Skogseth et al., 2005). In nearby areas, the bottom consists of gravel and mud-containing sand, sandy gravel and gravel.

Station 883 is located at the northeast coast of Svalbard, within the ice melting zone, and the water masses are clearly of Arctic origin. Sediment consists of mainly sandy mud.

2.3. Standards, reagents and materials

Uranium standard solution (1.000 g/L in 2 mol/L HNO_3, NIST, Gaithersburg, MD) was used after dilution as a standard for ^{238}U measurement. All reagents used in this work were of analytical grade and prepared using ultra-pure water (18 MΩ·cm). UTEVA resin (100–150 μm particle size, Triskem International, Bruz, France) was packed in 2-mL Econo-Columns (0.7 cm i.d. × 5 cm length, Bio-Rad Laboratories Inc., Hercules, CA) for the chromatographic purification of uranium. $FeCl_3$ solution (0.05 g/mL of Fe) was pre-purified by passing through a UTEVA column to remove any trace amount of uranium. The detailed preparation procedure was reported elsewhere (Qiao et al., 2015).

Table 1
Sample information.

Station ID	Sampling date	Latitude (°N)	Longitude (°E)	Echo depth (m)	Seawater temperature (°C)		Seawater salinity		Length of core (cm)	Sedimentation rate reported (mm/y)	Reference station	Sedimentation rate based on ^{236}U and ^{233}U data in this work (mm/y)
					Surface	Bottom	Surface	Bottom				
773	16/08/2015	70.65	32.30	289	10.45	3.03	34.23	34.69	14	0.6	Mareano ID-R1225 (70.47°N, 31.72°E), NGU report 2015–038	1.0
800	22/08/2015	74.88	16.86	285	7.72	3.95	34.95	35.05	15.5	1.1	Mareano ID-R1695 (74.81°N, 17.64°E), NGU report 2020–024	2.0
808	26/08/2015	77.61	13.42	147	3.25	3.69	30.70	35.02	10	1.7	Mareano ID-R1823 (77.69°N, 11.25°E), NGU report 2019–027	1.5
834	02/09/2015	75.26	37.06	175	5.70	0.57	34.87	35.03	12	1.4	Average of Mareano ID-R1776 (74.68°N, 36.10°E) and Mareano ID-R1819 (76.30°N, 36.62°E) in NGU report 2018–018	1.5
848	06/09/2015	77.30	19.58	162	1.27	−1.83	33.45	35.05	15	1.9	Average of Mareano ID-R1676 (76.12°N, 17.77°E) in NGU report 2018–001 and Station SB-3 (76.58°N, 20.00°E) in Heldal et al., 2002 (Heldal et al., 2002)	1.2
883	22/09/2015	79.36	27.36	293	0.61	0.65	33.82	34.83	10	1.0	Estimation in this work	0.8

2.4. Analytical method for determination of ^{137}Cs

The ^{137}Cs activity concentration in the samples was determined by gamma spectrometry at IMR using the 661.7 keV gamma peak. The analytical method is accredited under the standard ISO 17025. The calibration and validation sources are traceable to national standards (Eckert&Ziegler 1404-79-01 and 102166A). The samples (varying from 46.0 to 72.5 g dry weight) after homogenization were transferred to 60 mL polypropylene (PP) counting geometries. Two low-background ORTEC High Purity Germanium (HPGe) detector systems were used for ^{137}Cs measurement, i.e., an N-type coaxial HPGe-detector (model no. GMX-M5970P–S) with preamplifier (model no. 257 N) equipped with X-Cooler electric cryostat cooling system and DSPEC multichannel analyser; and a P-type coaxial HPGe-detector (model no. GEM-S8530P4-RB) with preamplifier (model no. A257P) equipped with X-Cooler III electric cryostat cooling system and DSPEC-50 multichannel analyser. Relative efficiencies of the two detectors were 47 % and 52 % at 1.33 MeV, respectively. Counting times varied from approximately 59,000 to 404,000 s. Analytical uncertainties are given as expanded uncertainties in the results using a coverage factor of k = 1, including uncertainties in sample preparation, calibration standards, calibration methods, counting statistics and background correction.

2.5. Analytical methods for determination of U isotopes in sediment

The radiochemical method used for uranium isotopes determination in sediment was modified based on our earlier study (Qiao et al., 2015). 1–10 g of each sample was ashed overnight at 450 °C in a muffle oven. 60–100 mL of *aqua regia* were added to leach the sample on a hotplate for 30 min at 150 °C followed by 2 h at 200 °C. The leachate was weighed and an aliquot was taken for direct measurement of ^{238}U after 10,000 times dilutions with 0.5 M HNO_3 by a triple quadrupole inductively coupled plasmas mass spectrometry (ICP-QQQ 8800, Agilent). The ICP-QQQ instrument was equipped with an Xt-skimmer core and a concentric nebuliser under hot plasma conditions. The typical operating conditions of the instrument have been given elsewhere (Qiao and Xu, 2018).

To the remaining leachate, 10 % $NH_3{\cdot}H_2O$ was slowly added to adjust the pH to 8–9. The sample was centrifuged at 3000 rpm for 10 min to discard the supernatant. The residue was dissolved with concentrated HNO_3 to a final concentration of 3 mol/L HNO_3. The sample solution was loaded onto a 2-mL UTEVA column which was preconditioned with 20 mL of 3 mol/L HNO_3. The UTEVA column was rinsed with 40 mL of 3 mol/L HNO_3, followed by 20 mL of 6 mol/L HCl. Uranium was finally eluted with 10 mL of 0.025 mol/L HCl.

A 100-μL aliquot of uranium eluate was taken and measured for ^{238}U after 1000–10,000 times dilution to calculate the chemical yield of uranium. To the remaining uranium eluate, 2 mg of Fe (as purified $FeCl_3$ solution) was added, and the sample was adjusted to pH > 9 with 25 % $NH_3{\cdot}H_2O$ to co-precipitate uranium. The precipitate was dried at 100 °C in an oven and baked for 8 h at 700 °C in a furnace. The sample was pressed into aluminium sputter target holders for the AMS measurement of $^{236}U/^{238}U$ and $^{233}U/^{236}U$ by the 3-MV tandem accelerator facility VERA (Vienna Environmental Research Accelerator) at the University of Vienna, Austria. The AMS measurement details for $^{236}U/^{238}U$ and $^{233}U/^{236}U$ have been reported elsewhere (Qiao et al., 2021). The concentration of ^{236}U or ^{233}U in each sediment is obtained by multiplying the $^{236}U/^{238}U$ or $^{233}U/^{238}U$ atomic ratio measured by AMS with the ^{238}U concentration measured by ICP-QQQ.

3. Results and discussion

3.1. ^{236}U, ^{233}U and ^{137}Cs concentration and inventory

The overall results obtained in this work are summarized in Table 2. Depth profiles of ^{236}U and ^{233}U concentrations (atom/kg), together with ^{137}Cs concentrations (Bq/kg), are shown in Fig. 2. The maximum ^{236}U concentration ((16.2 ± 0.16) × 10^9 atoms/kg) obtained in this work is similar to that in Philippine Sea sediment ((16.3 ± 0.07) × 10^9 atoms/kg, excluding the top 0–6 cm affected by terrestrial input) (Qiao et al., 2022), but a factor of 3 and 5 lower than those in the Japan Sea ((48.6 ± 0.76) × 10^9 atoms/kg) (Sakaguchi et al., 2012) and Atlantic Ocean sediments ((86 ± 6) × 10^9 atoms/kg) (Villa-Alfageme et al., 2018), respectively.

The cumulative areal inventories of ^{236}U and ^{233}U for the six investigated sites in the Barents Sea are in the range of (3.50–12.7) × 10^{11} atom/m^2 and (4.92–21.2) × 10^9 atom/m^2, respectively. ^{236}U inventory originating directly from global fallout was estimated to be (1.78 ± 0.05) × 10^{13} atom/m^2 based on Japanese soil data (Sakaguchi et al., 2010), which is more than one order of magnitude higher than our results. Sakaguchi et al. (2012) have also observed nearly one order of magnitude lower ^{236}U inventory ((1.50 ± 0.13) × 10^{11} atom/m^2) in the bottom sediment of the Japan Sea compare to that in the water column ((1.37 ± 0.09) × 10^{13} atom/m^2), indicating a very limited scavenge (ca. 1.1 %) of anthropogenic uranium from water column into sediment in the open ocean. This is reasonable as uranium is highly soluble in the open ocean where ≤2 % of the total amount of dissolved uranium in surface waters is estimated to adsorbed by particles (IAEA, 2004). A ^{236}U inventory of 1.04 × 10^{12} atom/m^2, which is comparable to the maximum value obtained in this work (1.27 × 10^{12} atom/m^2), was found in the sediment from the North Atlantic Ocean Porcupine Abyssal Plain site, which

was excluded from the impact of the European reprocessing plants (Villa-Alfageme et al., 2018). Associated with higher particle load and sedimentation rate, a higher areal cumulative inventory of ^{236}U compared to this work was reported in a sediment core from the Philippine Sea ((2.79 ± 0.20) × 10^{12} atom/m^2). Up to date, the highest sedimentary ^{236}U inventory in the range of (3.16–3.53) × 10^{13} atom/m^2 was reported for the Baltic Sea (Lin et al., 2021), which was related to the significant input of ^{236}U from the two European reprocessing plants.

A recent study estimated the direct deposition of global fallout ^{233}U in the 50°N latitude belt to be ((1.15 ± 0.10) × 10^{11} atom/m^2 based on the published peat core data (Lin et al., 2021). ^{233}U inventories in the Barents Sea sediment obtained in this work are about 4–19 % of the directly deposited global fallout inventory. Data on the sedimentary inventory of anthropogenic ^{233}U is very limited. So far, the only available ^{233}U sedimentary inventories were reported for the Philippine Sea (Qiao et al., 2022) and Baltic Sea (Lin et al., 2021), with corresponding values of (3.12 ± 0.41) × 10^{10} atom/m^2 and (2.42–2.85) × 10^{11} atom/m^2, respectively. All these reported ^{233}U inventories are higher than those ((4.92–21.2) × 10^9 atom/m^2) obtained in this work, especially for the Baltic Sea sediments whose ^{233}U inventories are 1–2 order of magnitude higher than those in the Barents Sea. As global fallout of atmospheric nuclear weapons testing is regarded as the sole source of anthropogenic ^{233}U in the environment, lower ^{233}U inventories in the Barents Sea indicate less significant scavenging of global fallout uranium into bottom sediments here compared to other areas. This is a consequence of lower depositional flux from global fallout in higher latitude belts and less particle load in the Barents Sea compared to the continental slope of the Philippine Sea and semi-closed Baltic Sea. Besides, anoxic conditions in Baltic Sea sediments as well as additional ^{233}U inputs from the large Baltic catchment areas make the uranium deposition in the Baltic seabed even more pronounced compared to other marine systems. Taking the average inventories of ^{236}U ((8.08 ± 2.93) × 10^{11} atom/m^2) and ^{233}U ((1.08 ± 0.56) × 10^{10} atom/m^2) as representative for the Barents Sea (1.6 million km^2), the total quantities of ^{236}U and ^{233}U deposited in the bottom sediment were estimated to be 507 ± 184 g and 7 ± 3 g. They are negligible compared to the total direct deposition of ^{236}U and ^{233}U from global fallout (mainly on the Northern Hemisphere with an area of 255 million km^2) into the Barents Sea, which are 6000 g (1000 kg of ^{236}U global inventory × 1.6 million km^2/255 million km^2) and 40–90 g (7–15 kg of ^{233}U global inventory (Lin et al., 2021) × 1.6 million km^2/255 million km^2), respectively.

Significant correlation between ^{236}U and ^{233}U inventory at the six sampling sites in the Barents Sea was observed (r = 0.90, p < 0.05, n = 6); whereas correlation between inventories of ^{137}Cs and ^{236}U (r = 0.47, n = 6) or between ^{137}Cs and ^{233}U (r = 0.54, n = 6) is not significant. ^{137}Cs inventory in this work range in 103–428 Bq/m^2, in the higher end compared to ^{137}Cs inventories (13–304 Bq/m^2) reported for sediments in the Japan Sea which are primarily originating from global fallout (Otosaka et al., 2006). That potentially indicates additional input of ^{137}Cs from other sources besides global fallout, such as the Chernobyl accident and releases from European reprocessing plants. Observations from Norway's national monitoring programme Radioactivity in the Marine Environment (RAME; www.dsa.no) indicate that the Norwegian coastal current is still supplied with Chernobyl contamination from land areas that received Chernobyl fallout (Skjerdal et al., 2020).

3.2. Anthropogenic uranium sources as determined by ^{233}U/^{236}U atomic ratios

^{233}U/^{236}U atomic ratios were applied in a two end-member model to calculate the contribution of ^{236}U from global fallout and nuclear reactor. The proportion (P_r) of reactor-^{236}U can be obtained using Eq. (1), with detailed derivation reported elsewhere (Qiao et al., 2020).

$$P_r, \% = \frac{N_{236,\,r}}{N_{236,\,r} + N_{236,\,f}} = \frac{R_f - R_s}{R_f - R_r} \quad (1)$$

where $N_{236,\,f}$ and $N_{236,\,r}$ refer to the atomic number of ^{236}U from global fallout and nuclear reactor, respectively; R_s, R_f and R_r respectively represent the ^{233}U/^{236}U atomic ratio of the sample, global fallout and nuclear reactor. Here we assume R_f = (1.40 ± 0.15) × 10^{-2} and R_r = 1 × 10^{-7}. Uncertainties of P_r were calculated based on the law of uncertainty propagation detailed in our earlier study (Lin et al., 2022a; Lin et al., 2022b).

Thereby, ^{236}U concentrations associated with nuclear reactor and global fallout input are calculated for the sediment depth profiles as demonstrated in Fig. 3. The overall ^{233}U/^{236}U atomic ratios obtained in this work vary within (0.18–4.30) × 10^{-2}. The integrated ^{233}U/^{236}U atomic ratios ((0.98–1.67) × 10^{-2}) based on the ^{233}U and ^{236}U inventories in the six sediment cores are close to the representative global fallout value (1.40 ± 0.15) × 10^{-2}, implying prominent impact of global fallout ^{236}U in the study sites of the Barents Sea. Based on the nuclear reactor derived ^{236}U concentration in the sediment cores (Fig. 3), the cumulative areal inventories for reactor-^{236}U are calculated to be in the range of (3.88–27.4) × 10^{10} atom/m^2, with an average of (1.63 ± 1.00) × 10^{11} atom/m^2. The highest reactor-^{236}U inventory was found at station 773 ((2.74 ± 1.71) × 10^{11} atom/m^2), whereas the lowest reactor-^{236}U inventory (3.88 ± 0.41) × 10^{10} atom/m^2) was observed at the east coast of Svalbard (station 883).

It is very difficult to relate the reactor ^{236}U input to any local radioactive contamination in the Barents Sea and its surrounding area, e.g., Komsomolets. Though elevated levels of ^{137}Cs have been reported in seawater collected inside a ventilation pipe of Komsomolets and close to the wreck (collected 1–3 m or so above the ventilation pipe), no significant elevation in ^{137}Cs concentration in sediments around the wreck has been measured (Gwynn et al., 2018; Skjerdal et al., 2020). No elevated concentrations of Pu isotopes, ^{241}Am or ^{238}U have been observed around Komsomolets either (Flo, 2014). In contrast to ^{137}Cs, which is relatively volatile, actinides (e.g., uranium, plutonium and americium) released from the Chernobyl accident were hardly reported in the Barents Sea marine environment (Baxter et al., 1995; Gwynn et al., 2012). Thus, the most likely source of reactor ^{236}U in the Barents Sea is from the European nuclear reprocessing facilities LH and SF transported northwards by the NCC and Atlantic water.

3.3. Temporal and spatial variations of ^{236}U, ^{233}U and ^{137}Cs deposition

Age-depth correlations for the six sediment cores were obtained based on reported sedimentation rates (Table 1) for locations nearby those investigated in this work. In most cases, the first occurrences of ^{233}U and ^{236}U peaks are observed in the 1960s (Fig. S1). In some cases, the increase of ^{236}U concentrations continued until the late 1990s or 2000s, e.g., in stations 773, 848 and 883. We appreciate the large uncertainty in the age-depth calculation based on the sedimentation rate reported for adjacent locations in earlier studies. For example, ^{233}U and ^{236}U peaks were observed in sediment layers formed before 1920 in the sediment core from station 800, which is clearly not the case. This implies that instead of relying on previously estimated sedimentation rates, we could use the first peaks of ^{233}U and ^{236}U to anchor the period of 1960s in the sediment core.

There is a significant correlation (r ranging within 0.56–0.95, p < 0.05, n ranging within 10–13) between the temporal distribution trends of ^{233}U and ^{236}U concentrations except for core 834, whereas the ^{137}Cs seems significantly correlated to ^{236}U temporal distribution only in sediment cores 773 (r = 0.72, p < 0.01, n = 12) and 883 (r = 0.91, p < 0.01, n = 10). This might be related to different input functions between ^{137}Cs and anthropogenic uranium, as well as their different physical-chemical properties along their transport pathways (Ashraf et al., 2014; Klinkhammer and Palmer, 1991). A sediment input function for ^{137}Cs in the Barents Sea was constructed by Smith et al. (Smith et al., 1995) based on the historical record of ^{137}Cs concentrations measured in Arctic Ocean surface waters from a region (71–73°N, 20–30°E) where Norwegian Sea water is transported into the Barents Sea (Kershaw and Baxter, 1995). Although the data exhibit a fallout peak in the 1960s, a larger signal is evident in the 1980s associated with maximal Sellafield releases of ^{137}Cs in the mid-1970s into the Irish Sea, with a water transit time of 5 to 6 years between the Irish, North and Norwegian Seas (Livingston and Killworth, 1988) and/or contamination from Chernobyl accident. Higher ^{137}Cs input in the

Table 2
Overall analytical results for ^{137}Cs, ^{236}U concentrations and ^{233}U/^{236}U ratios in the sediment core.

Station ID	Depth (cm)	Age (y)	Bulk density (g/cm^3)	^{137}Cs concentration (Bq/kg)		^{137}Cs inventory (Bq/m^2)		^{236}U/^{238}U Atomic ratio		^{236}U concentration (atom/kg)		^{233}U/^{236}U atomic ratio		^{233}U/^{238}U atomic ratio		^{233}U concentration (atom/kg)		^{236}U inventory (atom/m^2)		^{233}U inventory (atom/m^2)		Pr (%)	
				Val.	Un.	Val.	Un.	Val.	Un.	Val.	Un.	Val.	Un.	Val.	Un.	Val.	Un.	Val.	Un.	Val.	Un.	Val.	Un.
773	0–1	2006.7	0.767	1.2	0.3	8.8	2.3	2.14E−09	1.00E−10	6.49E+09	3.10E+08	1.49E−02	2.48E−03	3.18E−11	5.10E−12	9.64E+07	1.55E+07	4.98E+10	2.38E+09	7.40E+08	1.19E+08	0.0	21.1
	1–2	1990.0	0.864	2.2	0.3	19.1	3.0	2.78E−09	9.40E−11	6.35E+09	2.19E+08	2.73E−02	2.68E−03	7.60E−11	7.00E−12	1.74E+08	1.60E+07	5.48E+10	1.89E+09	1.50E+09	1.38E+08	0.0	28.4
	2–3	1973.3	0.970	2.8	0.3	27.2	2.7	3.55E−09	1.70E−10	1.40E+10	6.87E+08	8.59E−03	1.68E−03	3.05E−11	5.80E−12	1.21E+08	2.29E+07	1.36E+11	6.66E+09	1.17E+09	2.22E+08	38.6	13.7
	3–4	1956.7	0.990	2.6	0.3	25.7	3.0	2.95E−09	1.40E−10	1.30E+10	6.16E+08	1.05E−02	2.23E−03	3.09E−11	6.40E−12	1.36E+08	2.81E+07	1.28E+11	6.09E+09	1.34E+09	2.78E+08	25.2	17.8
	4–5	1940.0	1.035	3.5	0.4	36.1	3.8	2.73E−09	1.20E−10	1.05E+10	4.72E+08	9.63E−03	1.25E−03	2.63E−11	3.20E−12	1.01E+08	1.23E+07	1.09E+11	4.89E+09	1.05E+09	1.28E+08	31.2	11.6
	5–6	1923.3	1.076	3.1	0.2	33.3	2.0	2.22E−09	1.10E−10	9.12E+09	4.55E+08	1.45E−02	2.41E−03	3.21E−11	5.10E−12	1.32E+08	2.10E+07	9.82E+10	4.90E+09	1.42E+09	2.26E+08	0.0	20.4
	6–7	1906.7	1.133	2.0	0.3	23.0	3.3	1.18E−09	5.10E−11	4.97E+09	2.15E+08	1.05E−02	1.84E−03	1.24E−11	2.10E−12	5.22E+07	8.84E+06	5.62E+10	2.43E+09	5.91E+08	1.00E+08	24.9	15.4
	7–8	1890.0	1.171	0.7	0.3	8.0	3.7	7.44E−10	1.50E−11	3.84E+09	1.17E+08	6.95E−03	7.52E−04	5.17E−12	5.50E−13	2.67E+07	2.84E+06	4.49E+10	1.37E+09	3.12E+08	3.32E+07	50.4	7.6
	8–9	1873.3	1.196	<0.5	–	–	–	7.38E−10	5.60E−11	3.87E+09	3.13E+08	3.20E−03	5.94E−04	2.36E−12	4.00E−13	1.24E+07	2.10E+06	4.63E+10	3.74E+09	1.48E+08	2.51E+07	77.2	4.9
	9–10	1856.7	1.219	<0.6	–	–	–	6.93E−10	1.30E−10	3.80E+09	7.21E+08	1.23E−02	1.09E−02	8.53E−12	7.40E−12	4.67E+07	4.05E+07	4.63E+10	8.79E+09	5.70E+08	4.94E+08	12.1	78.4
	10–12	1831.7	1.234	<0.5	–	–	–	2.88E−10	5.60E−11	1.33E+09	2.59E+08	1.84E−03	1.27E−03	5.29E−13	3.50E−13	2.44E+06	1.61E+06	3.27E+10	6.39E+09	6.01E+07	3.98E+07	86.9	9.2
	12–14	1798.3	1.226	<0.5	–	–	–	3.36E−10	2.60E−11	2.78E+09	2.19E+08	4.08E−03	1.12E−03	1.37E−12	3.60E−13	1.13E+07	2.97E+06	6.81E+10	5.37E+09	2.78E+08	7.29E+07	70.9	8.6
Areal inventory						181.3	23.9											8.71E+11	5.49E+10	9.18E+09	1.88E+09		
Integrated ^{233}U/^{236}U atomic ratio														1.05E−02	2.25E−03							24.7	18.0
800	0–1	2010.5	0.714	3.6	0.4	25.5	2.7	3.66E−09	1.60E−10	7.31E+09	6.89E+08	9.95E−03	1.83E−03	3.64E−11	6.50E−12	7.27E+07	1.30E+07	5.22E+10	4.92E+09	5.19E+08	9.27E+07	29.0	15.1
	1–2	2001.4	0.761	2.6	0.3	20.1	2.4	4.26E−09	1.90E−10	7.99E+09	1.00E+09	4.30E−02	4.01E−03	1.83E−10	1.50E−11	3.43E+08	2.81E+07	6.08E+10	7.64E+09	2.61E+09	2.14E+08	0.0	43.6
	2–3	1992.3	0.781	2.3	0.4	18.0	3.2	3.72E−09	5.80E−10	7.35E+09	1.29E+09	1.76E−02	6.80E−03	6.53E−10	2.30E−11	1.29E+08	4.55E+07	5.74E+10	1.01E+10	1.01E+09	3.55E+08	0.0	50.4
	3–4	1983.2	0.808	2.5	0.3	20.3	2.7	4.06E−09	1.60E−10	9.00E+09	8.92E+08	1.20E−02	1.81E−03	4.89E−11	7.10E−12	1.08E+08	1.57E+07	7.27E+10	7.21E+09	8.75E+08	1.27E+08	14.0	15.9
	4–5	1974.1	0.846	3.2	0.2	27.4	1.7	2.43E−09	3.00E−10	6.29E+09	1.19E+09	2.46E−02	3.81E−03	5.97E−11	5.60E−12	1.55E+08	1.45E+07	5.33E+10	1.01E+10	1.31E+09	1.23E+08	0.0	33.1
	5–6	1965.0	0.860	4.0	0.3	34.1	2.8	2.94E−09	1.40E−09	7.68E+09	3.78E+09	9.42E−03	5.43E−03	2.77E−11	9.00E−12	7.23E+07	2.35E+07	6.60E+10	3.25E+10	6.22E+08	2.02E+08	32.7	39.5
	6–7	1955.9	0.882	3.9	0.4	34.7	3.3	3.15E−09	3.30E−10	8.88E+09	1.57E+09	8.38E−03	2.21E−03	2.64E−11	6.40E−12	7.44E+07	1.80E+07	7.83E+10	1.39E+10	6.56E+08	1.59E+08	40.1	17.1
	7–8	1946.8	0.898	4.4	0.3	39.8	2.7	3.17E−09	9.30E−11	8.55E+09	1.01E+09	1.17E−02	2.42E−03	3.72E−11	7.60E−12	1.00E+08	2.05E+07	7.68E+10	9.05E+09	9.01E+08	1.84E+08	16.2	19.5
	8–9	1937.7	0.909	4.3	0.3	38.8	3.1	4.11E−09	1.00E−10	1.26E+10	1.61E+09	1.24E−02	1.16E−03	5.09E−11	4.60E−12	1.56E+08	1.41E+07	1.15E+11	1.46E+10	1.42E+09	1.28E+08	11.5	12.6
	9–10	1928.6	0.925	4.3	0.2	39.5	1.9	3.89E−09	3.80E−10	1.23E+10	1.76E+09	1.43E−02	3.39E−03	5.58E−11	1.20E−11	1.77E+08	3.80E+07	1.14E+11	1.63E+10	1.63E+09	3.51E+08	0.0	26.6

	10–12	1915.0	0.918	3.0	0.3	54.6	6.1	4.80E−09	1.50E−10	1.62E+10	1.64E+09	1.94E−02	1.50E−03	9.29E−11	6.60E−12	3.14E+08	2.23E+07	2.98E+11	3.02E+10	5.77E+09	4.10E+08	0.0	18.3
	12–14	1896.8	0.967	1.7	0.3	32.7	5.3	2.46E−09	3.00E−10	8.32E+09	1.29E+09	1.31E−02	2.46E−03	3.23E−11	4.60E−12	1.65E+08	2.35E+07	1.61E+11	2.50E+10	3.20E+09	4.55E+08	6.2	20.3
	14–15.5	1880.9	1.048	0.8	0.3	12.0	4.4	7.87E−10	4.60E−11	4.02E+09	2.35E+08	6.39E−03	1.15E−03	5.03E−12	8.60E−13	4.49E+07	7.68E+06	6.33E+10	3.70E+09	7.06E+08	1.21E+08	54.3	9.6
Areal inventory						397.4	42.5											1.27E+12	1.85E+11	2.12E+10	2.92E+09		
Integrated $^{233}U/^{236}U$ atomic ratio														1.67E−02	3.36E−03							0.0	27.2
808	0–1	2012.1	0.606	4.5	0.4	27.0	2.7	3.16E−09	4.70E−10	6.41E+09	9.59E+08	2.46E−02	2.00E−02	7.76E−11	6.20E−11	1.57E+08	1.26E+08	3.88E+10	5.81E+09	9.53E+08	7.62E+08	0.0	143.8
	1–2	2006.2	0.749	4.6	0.3	34.1	1.9	1.62E−09	2.20E−10	3.72E+09	5.10E+08	2.47E−02	9.27E−03	4.00E−11	1.40E−11	9.20E+07	3.22E+07	2.79E+10	3.82E+09	6.89E+08	2.41E+08	0.0	68.9
	2–3	2000.3	0.835	5.3	0.4	44.1	3.5	2.29E−09	1.20E−10	6.70E+09	3.85E+08	8.34E−03	1.93E−03	1.91E−11	4.30E−12	5.59E+07	1.26E+07	5.60E+10	3.22E+09	4.67E+08	1.05E+08	40.4	15.2
	3–4	1994.4	0.887	5.3	0.4	46.9	3.9	2.23E−09	1.20E−10	7.18E+09	4.27E+08	1.62E−02	2.70E−03	3.62E−11	5.70E−12	1.16E+08	1.83E+07	6.36E+10	3.78E+09	1.03E+09	1.63E+08	0.0	22.9
	4–5	1988.5	0.927	5.6	0.4	51.9	4.1	2.15E−09	1.70E−10	7.21E+09	6.02E+08	1.20E−02	3.21E−03	2.57E−11	6.60E−12	8.62E+07	2.21E+07	6.68E+10	5.58E+09	7.99E+08	2.05E+08	14.6	24.7
	5–6	1982.6	0.953	5.9	0.3	56.1	2.5	2.93E−09	2.80E−10	1.00E+10	9.82E+08	1.39E−02	2.56E−03	4.08E−11	6.40E−12	1.40E+08	2.19E+07	9.55E+10	9.36E+09	1.33E+09	2.09E+08	0.5	21.2
	6–7	1976.8	0.966	5.5	0.5	53.4	4.5	3.49E−09	2.40E−10	1.16E+10	8.43E+08	1.46E−02	3.86E−03	5.11E−11	1.30E−11	1.70E+08	4.33E+07	1.12E+11	8.14E+09	1.64E+09	4.18E+08	0.0	29.8
	7–8	1970.9	0.990	4.9	0.5	48.7	4.5	3.09E−09	1.40E−10	1.11E+10	5.50E+08	1.70E−02	1.70E−03	5.25E−11	4.70E−12	1.88E+08	1.68E+07	1.10E+11	5.45E+09	1.86E+09	1.67E+08	0.0	17.8
	8–9	1965.0	1.030	4.1	0.4	42.0	4.4	2.69E−09	1.60E−10	9.86E+09	6.12E+08	1.90E−02	2.40E−03	5.12E−11	5.70E−12	1.88E+08	2.09E+07	1.02E+11	6.30E+09	1.93E+09	2.15E+08	0.0	22.5
	9–10	1959.1	1.086	2.2	0.4	23.6	4.3	1.76E−09	1.20E−10	6.87E+09	4.92E+08	1.03E−02	2.60E−03	1.81E−11	4.40E−12	7.07E+07	1.72E+07	7.46E+10	5.34E+09	7.68E+08	1.87E+08	26.5	20.1
Areal inventory						427.9	36.2											7.47E+11	5.68E+10	1.15E+10	2.67E+09		
Integrated $^{233}U/^{236}U$ atomic ratio														1.54E−02	3.76E−03							0.0	29.3
	0–1	2012.1	1.100	1.2	0.2	13.5	1.8	1.72E−09	1.80E−10	6.36E+09	6.69E+08	8.90E−03	1.78E−03	1.53E−11	2.60E−12	5.66E+07	9.61E+06	6.99E+10	7.36E+09	6.22E+08	1.06E+08	36.5	14.4
834	1–2	2006.2	0.897	1.7	0.3	15.0	2.7	1.89E−09	4.10E−11	9.79E+09	2.19E+08	1.21E−02	1.04E−03	2.29E−11	1.90E−12	1.19E+08	9.85E+06	8.78E+10	1.96E+09	1.06E+09	8.83E+07	13.5	11.9
	2–3	2000.3	0.778	1.5	0.3	11.9	2.0	1.82E−09	7.50E−11	9.38E+09	3.91E+08	8.63E−03	9.48E−04	1.57E−11	1.60E−12	8.09E+07	8.24E+06	7.30E+10	3.05E+09	6.30E+08	6.42E+07	38.4	9.5
	3–4	1994.4	0.817	1.9	0.3	15.3	2.2	1.70E−09	8.10E−11	8.71E+09	4.15E+08	1.05E−02	1.22E−03	1.78E−11	1.90E−12	9.11E+07	9.73E+06	7.11E+10	3.39E+09	7.44E+08	7.95E+07	25.2	11.9
	4–5	1988.5	0.853	1.6	0.2	13.6	1.3	1.55E−09	2.50E−10	8.63E+09	1.39E+09	1.84E−02	1.26E−03	2.85E−11	1.90E−11	1.59E+08	1.06E+08	7.36E+10	1.19E+10	1.35E+09	9.03E+08	0.0	91.1
	5–6	1982.6	0.868	1.2	0.2	10.8	2.2	1.33E−09	5.80E−11	8.28E+09	3.61E+08	1.05E−02	1.86E−03	1.40E−11	2.40E−12	8.72E+07	1.49E+07	7.19E+10	3.13E+09	7.56E+08	1.30E+08	24.8	15.5
	6–7	1976.8	0.886	0.6	0.3	5.0	2.3	1.23E−09	5.70E−11	7.24E+09	3.36E+08	1.24E−02	2.19E−03	1.52E−11	2.60E−12	8.95E+07	1.53E+07	6.42E+10	2.97E+09	7.93E+08	1.36E+08	11.7	18.3
	7–8	1970.9	0.889	0.8	0.2	7.1	1.6	1.15E−09	6.80E−11	6.58E+09	3.89E+08	1.49E−02	2.84E−03	1.71E−11	3.10E−12	9.79E+07	1.77E+07	5.85E+10	3.46E+09	8.70E+08	1.58E+08	0.0	23.2
	8–9	1965.0	0.905	0.7	0.1	6.4	1.1	9.93E−10	6.90E−11	6.04E+09	4.23E+08	3.77E−02	4.10E−03	3.74E−11	3.10E−12	2.27E+08	1.88E+07	5.46E+10	3.83E+09	2.06E+09	1.70E+08	0.0	41.1
	9–10	1959.1	0.915	0.5	0.1	4.8	1.3	2.32E−09	9.70E−10	1.32E+10	5.53E+09	3.78E−03	1.68E−03	8.76E−12	1.30E−12	4.98E+07	7.39E+06	1.21E+11	5.07E+10	4.56E+08	6.76E+07	73.0	12.3
	10–12	1950.3	0.891	<0.3	–	–	–	6.08E−10	3.70E−11	3.65E+09	2.59E+08	8.57E−03	2.36E−03	5.21E−12	1.40E−12	3.13E+07	8.41E+06	6.51E+10	4.61E+09	5.57E+08	1.50E+08	38.8	18.1
Areal inventory						103.3	18.6											8.10E+11	9.63E+10	9.90E+09	2.05E+09		
Integrated $^{233}U/^{236}U$ atomic ratio														1.22E−02	2.92E−03							12.7	22.8
848	0–1	2012.3	0.445	3.5	0.4	15.5	1.6	3.22E−09	3.90E−10	8.81E+09	1.07E+09	6.83E−03	2.53E−03	2.20E−11	7.70E−12	6.02E+07	2.11E+07	3.92E+10	4.76E+09	2.68E+08	9.38E+07	51.2	18.8
	1–2	2006.9	0.558	5.8	0.4	32.4	2.3	1.95E−09	1.20E−10	5.13E	3.16E	8.72E−03	2.27E−03	1.70E−11	4.30E−12	4.47E	1.13E	2.86E	1.76E	2.50E	6.31E	37.7	17.5

(continued on next page)

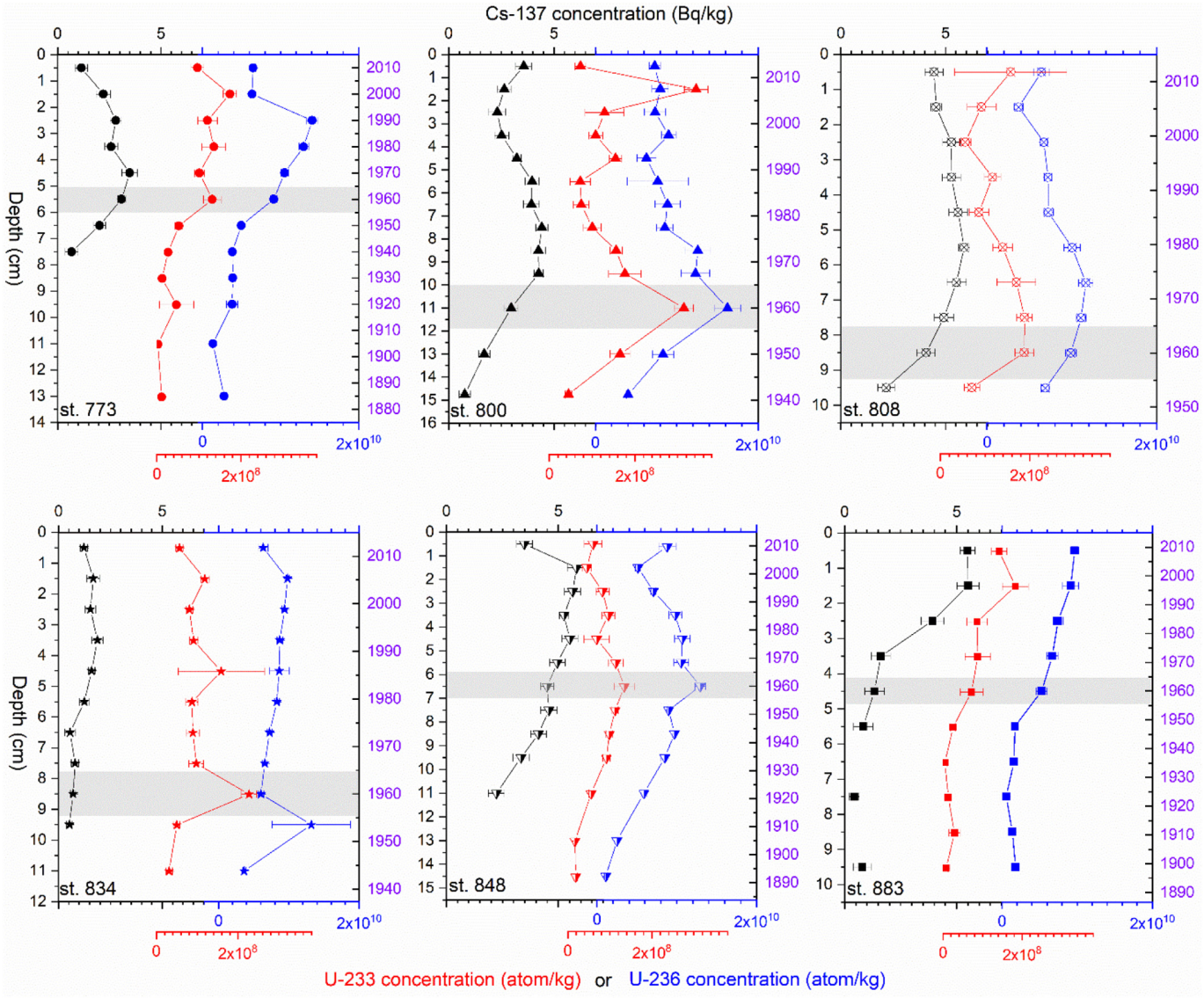

Fig. 2. ^{137}Cs, ^{236}U and ^{233}U concentrations in the sediment cores from the Barents Sea with age-depth correlation estimated based on ^{233}U-^{236}U data in this work (numbers in the right-Y axis are the years of corresponding sediment depths and the grey rectangles correspond to year 1960 ± 5 as identified by the onset of global fallout ^{233}U-^{236}U signal).

1980s was reflected in depth profiles of most investigated stations except for 773 and 800. The mismatch in the temporal deposition of ^{137}Cs for stations 773 and 800 (Fig. S1) again might be associated to uncertainties in sedimentation rate used in the age-depth calculation.

As the primary source of ^{236}U and ^{233}U in the Barents Sea sediment cores is from the global fallout. Therefore, we used the first occurrence of global fallout derived-^{236}U and ^{233}U peaks in each sediment profile to benchmark the age of the corresponding layer as 1960 ± 5, thereby the sedimentation rate (assumed to be constant) can be simply calculated using the onset depth divided by 55 (i.e., the interval between the sampling year 2015 and 1960). It can be seen from Table 1 that the sedimentation rate obtained from ^{236}U and ^{233}U data agree generally well with the reference stations, except for stations 773 and 800. The ^{236}U-^{233}U benchmarked age-depth profiles for stations 773 and 800 seem more reasonably to match the reported input function of ^{137}Cs in the Barents Sea (Fig. 2 and Fig. 3). The identified depth reflecting significant deposition of global fallout ^{233}U and ^{236}U in each sediment core is further validated by the corresponding ^{233}U/^{236}U atomic ratio, where in all cases the ^{233}U/^{236}U atomic ratios are comparable to the representative global fallout value of (1.40 ± 0.15) × 10^{-2} (Fig. 3). This highlights the potential of the anthropogenic ^{236}U-^{233}U pair as a robust tool for sediment dating and a useful complementary to e.g., the more traditional ^{210}Pb-dating method. We notice that there are still substantial ^{236}U and ^{233}U at the bottom of all six sediment profiles, this might imply that the uranium isotopes are moving down through the profile due to the high solubility of uranium in marine conditions.

Among the investigated stations, the highest ^{236}U and ^{233}U inventories were observed south of Svalbard (station 800) while the lowest were observed at station 883. Although all six stations are located far from the anticipated contamination sources, station 800 is the closest and station 883 is the farthest away. The reprocessing signal is transported to the area around station 883 with the North Atlantic Current and the West Spitsbergen Current, which is the northernmost extension of the North Atlantic Current. The West Spitsbergen Current splits in two north of Svalbard, and one branch flows eastwards. A small amount of the reprocessing signal in this branch may thereafter reach station 883 and enter the Barents Sea from the north. The contamination signal is probably diluted to lower levels on its way around Svalbard. Our results do not indicate that sea ice transport is an important process in the area around station 883.

The spatial distribution for anthropogenic uranium is somewhat different to ^{137}Cs, where the highest was observed in the western coast of

Svalbard (station 808) and the lowest in the central Barents Sea (station 834). Somewhat higher inventory at station 808 may be due to the presence of fine-grained sediments. Further, as this is an ice melting area, sea ice transport cannot be ruled out. Low levels at station 834 at the Central Bank may be related to little sedimentation of fine-grained sediments due to strong ocean currents. Earlier studies in the Barents Sea have confirmed a correlation between ^{137}Cs concentration and grain size, i.e. sediments with a high percentage of fine-grained particles have relatively high values of ^{137}Cs (Føyn and Sværen, 1997). Compared to ^{137}Cs, uranium is less particle-reactive, thus high fine-grain particle loads would enhance the accumulation of ^{137}Cs more significantly than uranium. This might be a factor to influence the spatial distribution variation between ^{137}Cs and anthropogenic uranium in the study region. Similar to the present study, Føyn and Sværen (1997) also observed the highest levels of ^{137}Cs in the Spitsbergen area. They suggested that phytoplankton in this biologically-productive polar front area actively transports ^{137}Cs to the sediments and thereby scavenges the water for radiocesium throughout the production period. However, an attempt to confirm this through laboratory experiments did not succeed (Heldal et al., 2001).

As discussed in our earlier work (Qiao et al., 2022), uranium can be transported from the water column into the bottom sediment by several pathways including direct deposition to sediments by fallout debris containing ^{236}U, scavenging of dissolved ^{236}U from the surface by sinking particles coupled with demineralization, reduction of uranium under anoxic condition followed by deposition to the seafloor, and in-situ production of ^{236}U from ^{240}Pu. In the Barents Sea, the deposition efficiency of global fallout ^{236}U may be associated to both particle load and the scavenging of dissolved uranium from the water column, whereas the reprocessing derived ^{236}U should be mostly in soluble form.

4. Conclusion

This work presents the first dataset on temporal and spatial distributions of ^{236}U and ^{233}U in the Barents Sea sediments, and provides insights on depositional history, source terms and transport pathways of anthropogenic uranium in the study region. The results reveal that the majority of anthropogenic uranium deposited in the Barents Sea bottom sediments originated from global fallout. The impact of the historical ^{236}U releases from

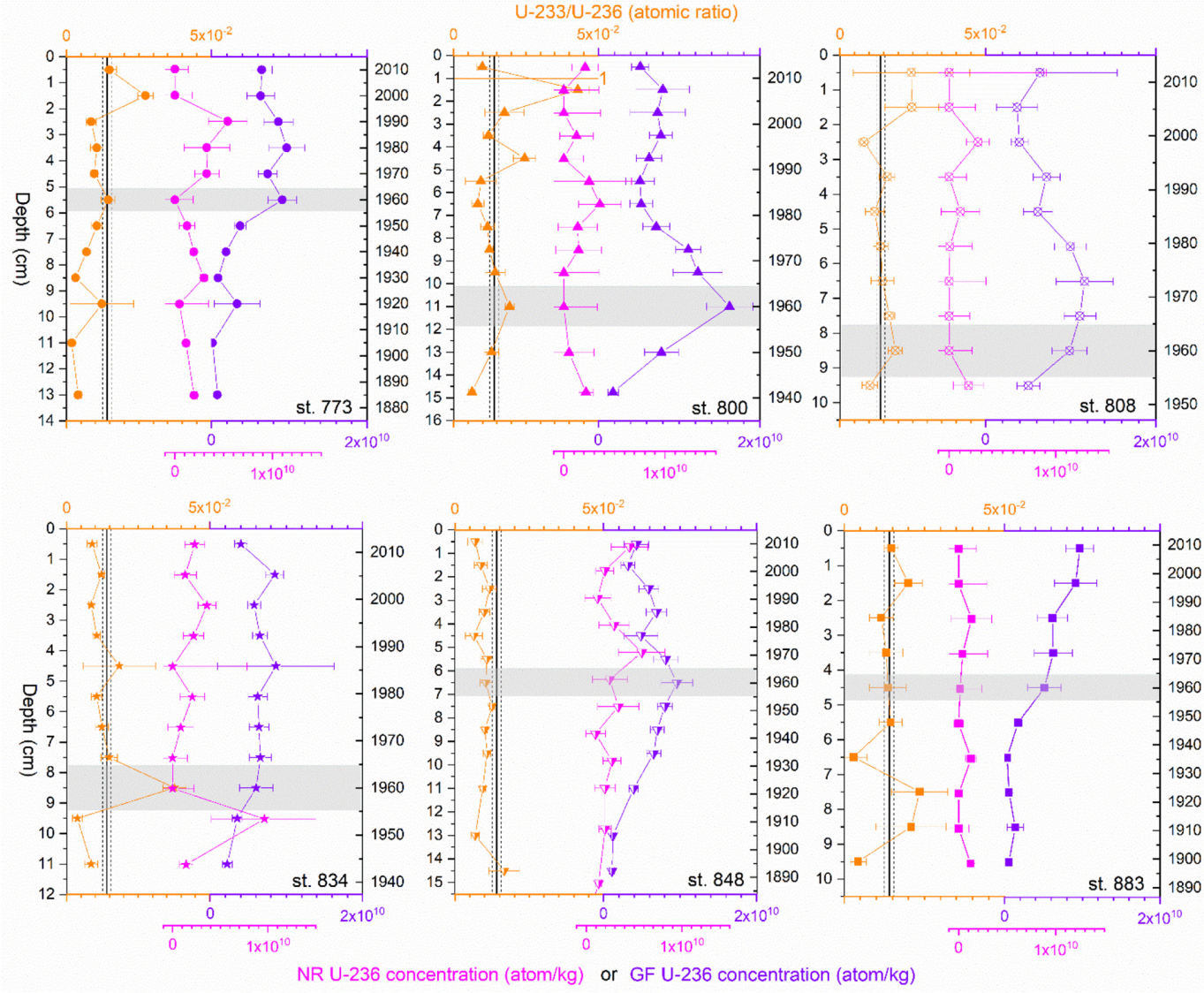

Fig. 3. ^{233}U/^{236}U atomic ratio and ^{236}U concentrations derived from global fallout (GF) and nuclear reactor (NR) in the sediment cores from the Barents Sea with age-depth correlation estimated based on ^{233}U-^{236}U data in this work (numbers in the right-Y axis are the years of corresponding sediment depths and the grey rectangles correspond to year 1960 ± 5 as identified by the onset of global fallout ^{233}U-^{236}U signal, the solid and dashed black lines demonstrates respectively the representative GF ^{233}U/^{236}U atomic ratio and the uncertainties, i.e. (1.40 ± 0.15) × 10^{-2}).

European reprocessing plants to the Barents Sea sediments is insignificant. Besides, the contribution of ^{236}U from local nuclear activities to the Barents Sea marine environment is unlikely to occur. Our work contributes to baseline knowledge in the oceanic tracer application of ^{236}U for studying the dynamics of the Atlantic-Arctic Ocean and associated climate changes. It also demonstrates that ^{236}U-^{233}U can be potentially used as benchmarks in the age-depth model for sediment dating.

CRediT authorship contribution statement

Jixin Qiao: Conceptualization, Resources, Methodology, Formal analysis, Data curation, Writing – original draft, Writing – review & editing. **Hilde Elise Heldal:** Investigation, Resources, Formal analysis, Data curation, Writing – review & editing. **Peter Steier:** Investigation, Methodology, Data curation, Resources, Writing – review & editing.

Data availability

Data will be made available on request.

Declaration of competing interest

The authors declare that they have no known competing financial interests or personal relationships that could have appeared to influence the work reported in this paper.

Acknowledgement

J. Qiao is grateful to support from colleagues in the Radioecology and Tracer Studies Section, Department of Environmental Engineering, Technical University of Denmark. Thanks are due to the crew of R/V "Johan Hjort" and Penny Lee Liebig (IMR) for assistance with sample collection and sample preparation and Kjell Bakkeplass for creating the map.

Appendix A. Supplementary data

Supplementary data to this article can be found online at https://doi.org/10.1016/j.scitotenv.2022.157503.

References

AMAP, 2015. AMAP Assessment: Radioactivity in the Arctic, AMAP Assessment.
Ashraf, M.A., Akib, S., Maah, M.J., Yusoff, I., Balkhair, K.S., 2014. Cesium-137: radiochemistry, fate, and transport, remediation, and future concerns. Crit. Rev. Environ. Sci. Technol. 44, 1740–1793. https://doi.org/10.1080/10643389.2013.790753.
Baxter, M.S., Fowler, S.W.W., Povinec, P.P., 1995. Observations on plutonium in the oceans. Appl. Radiat. Isot. 46, 1213–1223. https://doi.org/10.1016/0969-8043(95)00163-8.
Brown, J.E., Iospje, M., Kolstad, K.E., Lind, B., Rudjord, A.L., Strand, P., 2002. Temporal trends for 99Tc in norwegian coastal environments and spatial distribution in the Barents Sea. J. Environ. Radioact. 60, 49–60. https://doi.org/10.1016/S0265-931X(01)00095-9.
Carmack, E., Barber, D., Christensen, J., Macdonald, R., Rudels, B., Sakshaug, E., 2006. Climate variability and physical forcing of the food webs and the carbon budget on panarctic shelves. Prog. Oceanogr. 71, 145–181. https://doi.org/10.1016/j.pocean.2006.10.005.
Casacuberta, N., Masqué, P., Henderson, G., Bauch, D., Vockenhuber, C., Daraoui, A., Walther, C., Synal, H.A., Christl, M., Rutgers van-der-Loeff, M., 2016. First 236U data from the Arctic Ocean and use of 236U/238U and 129I/236U as a new dual tracer. Earth Planet. Sci. Lett. 440, 127–134. https://doi.org/10.1016/j.epsl.2016.02.020.
Castrillejo, M., Casacuberta, N., Christl, M., Vockenhuber, C., Synal, H.-A., García-Ibáñez, M.I., Lherminier, P., Sarthou, G., Garcia-Orellana, J., Masqué, P., 2018. Tracing water masses with 129I and 236U in the subpolar North Atlantic along the GEOTRACES GA01 section. Biogeosciences 15, 5545–5564. https://doi.org/10.5194/bg-15-5545-2018.
Castrillejo, M., Witbaard, R., Casacuberta, N., Richardson, C.A., Dekker, R., Synal, H.A., Christl, M., 2020. Unravelling 5 decades of anthropogenic 236U discharge from nuclear reprocessing plants. Sci. Total Environ. 717, 137094. https://doi.org/10.1016/j.scitotenv.2020.137094.
Dethleff, D., Nies, H., Harms, I.H., Karcher, M.J., 2000. Transport of radionuclides by sea-ice and dense-water formed in western Kara Sea flaw leads. J. Mar. Syst. 24, 233–248. https://doi.org/10.1016/S0924-7963(99)00088-3.
Durrant, C.B., Begg, J.D., Kersting, A.B., Zavarin, M., 2018. Cesium sorption reversibility and kinetics on illite, montmorillonite, and kaolinite. Sci. Total Environ. 610–611, 511–520. https://doi.org/10.1016/j.scitotenv.2017.08.122.
Falk-Petersen, S., Sargent, J.R., Henderson, J., Hegseth, E.N., Hop, H., Okolodkov, Y.B., 1998. Lipids and fatty acids in ice algae and phytoplankton from the marginal ice zone in the Barents Sea. Polar Biol. 20, 41–47. https://doi.org/10.1007/s003000050274.
Falk-Petersen, S., Hop, H., Budgell, W.P., Hegseth, E.N., Korsnes, R., Løyning, T.B., Børre Ørbæk, J., Kawamura, T., Shirasawa, K., 2000. Physical and ecological processes in the marginal ice zone of the northern Barents Sea during the summer melt period. J. Mar. Syst. 27, 131–159. https://doi.org/10.1016/S0924-7963(00)00064-6.
Flo, J.K., 2014. Radioactive Contamination in Sediments Near the Sunken Nuclear Submarine Komsomolets, SW of Bear Island in the Norwegian Sea. University of Bergen.
Føyn, L., Sværen, I., 1997. Distribution and sedimentation of radionuclides in the Barents Sea. ICES J. Mar. Sci. 54, 333–340. https://doi.org/10.1006/jmsc.1996.0174.
Gwynn, J.P., Heldal, H.E., Gäfvert, T., Blinova, O., Eriksson, M., Sværen, I., Brungot, A.L., Strålberg, E., Møller, B., Rudjord, A.L., 2012. Radiological status of the marine environment in the Barents Sea. J. Environ. Radioact. 113, 155–162. https://doi.org/10.1016/j.jenvrad.2012.06.003.
Gwynn, J.P., Nikitin, A., Shershakov, V., Heldal, H.E., Lind, B., Teien, H.C., Lind, O.C., Sidhu, R.S., Bakke, G., Kazennov, A., Grishin, D., Fedorova, A., Blinova, O., Sværen, I., Lee Liebig, P., Salbu, B., Wendell, C.C., Strålberg, E., Valetova, N., Petrenko, G., Katrich, I., Logoyda, I., Osvath, I., Levy, I., Bartocci, J., Pham, M.K., Sam, A., Nies, H., Rudjord, A.L., 2016. Main results of the 2012 joint norwegian-russian expedition to the dumping sites of the nuclear submarine K-27 and solid radioactive waste in Stepovogo Fjord, Novaya Zemlya. J. Environ. Radioact. 151, 417–426. https://doi.org/10.1016/j.jenvrad.2015.02.003.
Gwynn, J.P., Heldal, H.E., Flo, J.K., Sværen, I., Gäfvert, T., Haanes, H., Føyn, L., Rudjord, A.L., 2018. Norwegian monitoring (1990–2015) of the marine environment around the sunken nuclear submarine Komsomolets. J. Environ. Radioact. 182, 52–62. https://doi.org/10.1016/j.jenvrad.2017.11.015.
Hain, K., Steier, P., Froehlich, M.B., Golser, R., Hou, X., Lachner, J., Qiao, J., Quinto, F., Sakaguchi, A., 2020. 233U/236U signature allows to distinguish environmental emissions of civil nuclear industry from weapons fallout. Nat. Commun. 11, 1–11. https://doi.org/10.1038/s41467-020-15008.
Heldal, H.E., Stupakoff, I., Fisher, N.S., 2001. Bioaccumulation of 137Cs and 57Co by five marine phytoplankton species. J. Environ. Radioact. 57, 231–236. https://doi.org/10.1016/S0265-931X(01)00020-0.
Heldal, H.E., Varskog, P., Føyn, L., 2002. Distribution of selected anthropogenic radionuclides (137Cs, 238Pu, 239,240Pu and 214Am) in marine sediments with emphaisis on the Spitsbergen-Bear Island area. Sci. Total Environ. 293, 233–245.
IAEA, 2004. Sediment Distribution Coefficients and Concentration Factors for Biota in the Marine Environment. Tech. Reports Ser. No.422. 103.
Johannesen, E., Ingvaldsen, R.B., Bogstad, B., Dalpadado, P., Eriksen, E., Gjøsæter, H., Knutsen, T., Skern-Mauritzen, M., Stiansen, J.E., 2012. Changes in Barents Sea ecosystem state, 19702009: climate fluctuations, human impact, and trophic interactions. ICES J. Mar. Sci. https://doi.org/10.1093/icesjms/fss046.
Kershaw, P., Baxter, A., 1995. The transfer of reprocessing wastes from north-west Europe to the Arctic. Deep. Res. Part II 42, 1413–1448. https://doi.org/10.1016/0967-0645(95)00048-8.
Kershaw, P.J., McCubbin, D., Leonard, K.S., 1999. Continuing contamination of North Atlantic and Arctic waters by sellafield radionuclides. Sci. Total Environ. 237–238, 119–132. https://doi.org/10.1016/S0048-9697(99)00129-1.
Kershaw, P.J., Elise, H., Arne, K., Liv, A., 2004. Variability in the supply, distribution and transport of the transient tracer 99Tc in the NE. Atlantic 44, 55–81. https://doi.org/10.1016/j.jmarsys.2003.08.003.
Klinkhammer, G., Palmer, M., 1991. Uranium in the oceans: where it goes and why. Geochim. Cosmochim. Acta 55, 1799–1806. https://doi.org/10.1016/0016-7037(91)90024-Y.
Knies, J., Martinez, P., 2009. Organic matter sedimentation in the western Barents Sea region: terrestrial and marine contribution based on isotopic composition and organic nitrogen content. Nor. J. Geol. 89, 79–89.
Knies, J., Jensen, H.K.B., Finne, T.E., Lepland, A., M., S.O., 2006. Sediment composition and heavy metal distribution in Barents Sea surface samples: Results from Institute of Marine Research 2003 and 2004 cruises. NGU Rep. 2006 (067), 1–44.
Lin, G., Lin, M., Qiao, J., Sejr, M.K., Steier, P., Meire, L., Stedmon, C.A., 2022. Estimation of Atlantic water transit times in East Greenland fjords using a U- U tracer approach. Chem. Geol. 607, 121007. https://doi.org/10.1016/j.chemgeo.2022.121007.
Lin, M., Qiao, J., Hou, X., Dellwig, O., Steier, P., Hain, K., Golser, R., Zhu, L., 2021. 70-year anthropogenic uranium imprints of nuclear activities in Baltic Sea sediments. Environ. Sci. Technol. 55, 8918–8927. https://doi.org/10.1021/acs.est.1c02136.
Lin, M., Qiao, J., Hou, X., Steier, P., Golser, R., Schmidt, M., Dellwig, O., Hansson, M., Bäck, Ö., Vartti, V.P., Stedmon, C., She, J., Murawski, J., Aldahan, A., Schmied, S.A.K., 2022. Anthropogenic 236U and 233U in the Baltic Sea: distributions, source terms, and budgets. Water Res. 210. https://doi.org/10.1016/j.watres.2021.117987.
Livingston, H.D., Killworth, P.D., 1988. The use of cs and sr isotopes as tracers in the Arctic Mediterranean seas. Philos. Trans. RSoc. A Math. Phys. Eng. Sci. 325, 161–176. https://doi.org/10.1098/rsta.1988.0049.
Loeng, H., 1991. Features of the physical oceanographic conditions of the Barents Sea. Polar Res. 10, 5–18. https://doi.org/10.1111/j.1751-8369.1991.tb00630.x.
HELCOM MORS, n.d.HELCOM MORS Discharge database [WWW Document], n.d. URL https://helcom.fi/baltic-sea-trends/data-maps/databases/ (accessed 7.15.22).
Muz, M., Escher, B.I., Jahnke, A., 2020. Bioavailable environmental pollutant patterns in sediments from passive equilibrium sampling. Environ. Sci. Technol. 54, 15861–15871. https://doi.org/10.1021/acs.est.0c05537.
Naegeli, R.E., 2004. Calculation of the radionuclides in PWR spent fuel samples for SFR experiment planning, Sandia National Laboratories. Technical Report, Sandia National Laboratories, Albuquerque, NM 87123, USA.
Otosaka, S., Amano, H., Ito, T., Kawamura, H., Kobayashi, T., Suzuki, T., Togawa, O., Chaykovskaya, E.L., Lishavskaya, T.S., Novichkov, V.P., Karasev, E.V., Tkalin, A.V., Volkov, Y.N., 2006. Anthropogenic radionuclides in sediment in the Japan Sea:

distribution and transport processes of particulate radionuclides. J. Environ. Radioact. 91, 128–145. https://doi.org/10.1016/j.jenvrad.2006.09.001.
Qiao, J., Xu, Y., 2018. Direct measurement of uranium in seawater by inductively coupled plasma mass spectrometry. Talanta 183. https://doi.org/10.1016/j.talanta.2018.02.045.
Qiao, J., Hou, X., Steier, P., Nielsen, S., Golser, R., 2015. Method for 236U determination in seawater using flow injection extraction chromatography and accelerator mass spectrometry. Anal. Chem. 87, 7411–7417.
Qiao, J., Steier, P., Nielsen, S., Hou, X., Roos, P., Golser, R., 2017. Anthropogenic 236U in danish seawater: global fallout versus reprocessing discharge. Environ. Sci. Technol. 51, 6867–6876. https://doi.org/10.1021/acs.est.7b00504.
Qiao, J., Hain, K., Steier, P., 2020. First dataset of 236U and 233U around Greenland coast: a 5-year snapshot (2012–2016). Chemosphere 257, 127185.
Qiao, J., Zhang, H., Steier, P., Hain, K., Hou, X., Vartti, V.-P., Henderson, G., Eriksson, M., Aldahan, A., Possnert, G., Gloser, R., 2021. An unknown source of reactor radionuclides in the Baltic Sea revealed by multi-isotope fingerprints. Nat. Commun. 12, 823. https://doi.org/10.1038/s41467-021-21059-w.
Qiao, J., Ransby, D., Steier, P., 2022. Deciphering anthropogenic uranium sources in the equatorial Northwest Pacific margin. Sci. Total Environ. 806, 150482. https://doi.org/10.1016/j.scitotenv.2021.150482.
Sakaguchi, A., Kawai, K., Steier, P., Quinto, F., Mino, K., Tomita, J., Hoshi, M., Whitehead, N., Yamamoto, M., 2009. First results on 236U levels in global fallout. Sci. Total Environ. 407, 4238–4242. https://doi.org/10.1016/j.scitotenv.2009.01.058.
Sakaguchi, A., Kawai, K., Steier, P., Imanaka, T., Hoshi, M., Endo, S., Zhumadilov, K., Yamamoto, M., 2010. Feasibility of using 236U to reconstruct close-in fallout deposition from the Hiroshima atomic bomb. Sci. Total Environ. 408, 5392–5398. https://doi.org/10.1016/j.scitotenv.2010.07.073.
Sakaguchi, A., Kadokura, A., Steier, P., Takahashi, Y., Shizuma, K., Hoshi, M., Nakakuki, T., Yamamoto, M., 2012. Uranium-236 as a new oceanic tracer: a first depth profile in the Japan Sea and comparison with caesium-137. Earth Planet. Sci. Lett. 333, 165–170. https://doi.org/10.1016/j.epsl.2012.04.004.
Skjerdal, H., Heldal, H.E., Rand, A., Gwynn, J., Jensen, L.K., Volynkin, A., Haanes, H., Møller, B., Liebig, P.L., Gäfvert, T., 2020. Radioactivity in the Marine Environment 2015, 2016 and 2017. Results from the Norwegian Marine Monitoring Programme (RAME), DSA Report 2020:04.
Skogseth, R., Haugan, P.M., Jakobsson, M., 2005. Watermass transformations in storfjorden. Cont. Shelf Res. 25, 667–695. https://doi.org/10.1016/j.csr.2004.10.005.
Smith, J.N., Ellis, K.M., Naes, K., Dahle, S., Matishov, D., 1995. Sedimentation and mixing rates of radionuclides in Barents Sea sediments off Novaya Zemlya. Deep. Res. II 42, 1471–1493.
Steier, P., Bichler, M., Keith Fifield, L., Golser, R., Kutschera, W., Priller, A., Quinto, F., Richter, S., Srncik, M., Terrasi, P., Wacker, L., Wallner, A., Wallner, G., Wilcken, K.M., Maria Wild, E., 2008. Natural and anthropogenic 236U in environmental samples. Nucl. Inst. and Methods Phys. Res. B 266, 2246–2250.
UNSCEAR, 2000. Source and effect of ionzing raidation. United Nations Scientific Committee on the Effects of Atomic Radiation, New York.
Viinje, T., Kvambekk, Å.S., 1991. Barents Sea drift ice characteristics. Polar Res. 10, 59–68. https://doi.org/10.1111/j.1751-8369.1991.tb00635.x.
Villa-Alfageme, M., Chamizo, E., Santos-Arévalo, F.J., López-Gutierrez, J.M., Gómez-Martínez, I., Hurtado-Bermúdez, S., 2018. Natural and artificial radionuclides in a marine core. First results of 236U in North Atlantic Ocean sediments. J. Environ. Radioact. 186, 152–160. https://doi.org/10.1016/j.jenvrad.2017.10.001.
Villa-Alfageme, M., Chamizo, E., Kenna, T.C., López-Lora, M., Casacuberta, N., Chang, C., Masqué, P., Christl, M., 2019. Distribution of 236U in the U.S. GEOTRACES eastern Pacific zonal transect and its use as a water mass tracer. Chem. Geol. 517. https://doi.org/10.1016/j.chemgeo.2019.04.003.
Wefing, A.M., Christl, M., Vockenhuber, C., Rutgers van der Loeff, M., Casacuberta, N., 2019. Tracing Atlantic waters using 129I and 236U in the Fram Strait in 2016. J. Geophys. Res. Ocean. 124, 882–896. https://doi.org/10.1029/2018JC014399.
Winkler, S.R., Steier, P., Carilli, J., 2012. Bomb fall-out 236U as a global oceanic tracer using an annually resolved coral core. Earth Planet. Sci. Lett. 359–360, 124–130.
Yakovlev, E., Puchkov, A., 2020. Assessment of current natural and anthropogenic radionuclide activity concentrations in the bottom sediments from the Barents Sea. Mar. Pollut. Bull. 160. https://doi.org/10.1016/j.marpolbul.2020.111571.
Zaborska, A., Carroll, J., Pazdro, K., Pempkowiak, J., 2011. Spatio-temporal patterns of PAHs, PCBs and HCB in sediments of the western Barents Sea. Oceanologia 53, 1005–1026. https://doi.org/10.5697/oc.53-4.1005.